Rapid Communications

Magnetic anisotropy of the alkali iridate Na_2IrO_3 at high magnetic fields: Evidence for strong ferromagnetic Kitaev correlations

Sitikantha D. Das,[1,2] Sarbajaya Kundu,[3] Zengwei Zhu,[4,*] Eundeok Mun,[4,†] Ross D. McDonald,[4] Gang Li,[5,‡] Luis Balicas,[5] Alix McCollam,[6] Gang Cao,[7,8] Jeffrey G. Rau,[9,§] Hae-Young Kee,[9,10] Vikram Tripathi,[3,‖] and Suchitra E. Sebastian[1]

[1]*Cavendish Laboratory, University of Cambridge, J J Thomson Avenue, Cambridge CB3 0HE, United Kingdom*

[2]*Department of Physics, IIT, Kharagpur, Kharagpur 721302, India*

[3]*Department of Theoretical Physics, Tata Institute of Fundamental Research, Homi Bhabha Road, Colaba, Mumbai 400005, India*

[4]*Los Alamos National Laboratory, Los Alamos, New Mexico 87545, USA*

[5]*National High Magnetic Field Laboratory,1800 E. Paul Dirac Drive, Tallahassee, Florida 32310, USA*

[6]*High Field Magnet Laboratory (HFML - EMFL), Radboud University, 6525 ED, Nijmegen, The Netherlands*

[7]*Center for Advanced Materials and Department of Physics and Astronomy, University of Kentucky, Lexington, Kentucky 40506, USA*

[8]*Department of Physics, 390 UCB, University of Colorado, Boulder, Colorado 80309, USA*

[9]*Department of Physics, University of Toronto, Toronto, Ontario, Canada M5S 1A7*

[10]*Canadian Institute for Advanced Research/Quantum Materials Program, Toronto, Ontario, Canada MSG 1Z8*

(Received 15 September 2017; revised manuscript received 1 October 2018; published 1 February 2019)

The magnetic-field response of the Mott-insulating honeycomb iridate Na_2IrO_3 is investigated using torque magnetometry measurements in magnetic fields up to 60 T. A peak-dip structure is observed in the torque response at magnetic fields corresponding to an energy scale close to the zigzag ordering ($\approx$15 K) temperature. Using exact diagonalization calculations, we show that such a distinctive signature in the torque response constrains the effective spin models for these classes of Kitaev materials to ones with dominant ferromagnetic Kitaev interactions, while alternative models with dominant antiferromagnetic Kitaev interactions are excluded. We further show that, at high magnetic fields, long range spin correlation functions decay rapidly, pointing to a transition to a long-sought-after field-induced quantum spin liquid beyond the peak-dip structure, suggesting this to be a common feature of the family of Kitaev systems. Kitaev systems are thus revealed to be excellent candidates for field-induced quantum spin liquids, similar physics having been suggested in another Kitaev system α-$RuCl_3$.

DOI: 10.1103/PhysRevB.99.081101

The alkali iridates A_2IrO_3 (A=Na,Li), along with their celebrated 4*d* analog, α-$RuCl_3$ [1–13], have attracted much theoretical [14–34] and experimental [35–46] attention as promising candidates for realizing the physics of the honeycomb Kitaev model [47,48]. Interactions between the effective $j_{\text{eff}} = \frac{1}{2}$ pseudospins on every site of the two-dimensional hexagonal lattice in these strongly spin-orbit coupled materials have been described by a dominant Kitaev and other subdominant interactions such as Heisenberg [49] and symmetric off-diagonal exchange [18,38,42,49–51]. Notwithstanding the great progress made, the sign of the dominant Kitaev interaction remains a question of vital importance in ascertaining the correct physics in this class of materials [16,17,26,52,53]. The importance of the magnetic-field response in determining the same has been emphasized in multiple studies recently [54,55], and it has, indeed, been used to experimentally investigate the Kitaev material α-$RuCl_3$ [56]. Yet high magnetic-field studies has thus far been impracticable in Na_2IrO_3 because of the evidently higher energy scales involved. Here, we probe the physics of Na_2IrO_3 by using a combination of magnetometry studies in very high magnetic fields up to 60 T, and exact diagonalization calculations. We find a distinctive peak-dip structure in the experimental magnetic torque response at high magnetic fields, which we use to constrain the model description of Na_2IrO_3. By comparison with results of exact diagonalization calculations, we show that the nonmonotonic signature we find in magnetic torque measurements is uniquely captured by a model with a dominant ferromagnetic Kitaev exchange, but not one with an antiferromagnetic Kitaev counterpart. Crucially, instead of a stable zigzag ground state, expected over a wide region of phase space for a model with dominant antiferromagnetic Kitaev exchange [26,51], we find a finely tuned zigzag ground state in the model with a dominant ferromagnetic Kitaev exchange [15–17,35] to be of relevance to Na_2IrO_3. We find this zigzag ground state to give way to a quantum spin liquid state by magnetic-field tuning beyond the peak-dip feature. Intriguingly, a similar peak-dip structure in the anisotropic magnetization was also

*Now at National High Magnetic Field Center and School of Physics, Huazhong University of Science and Technology, Wuhan 430074, China.

†Now at Department of Physics, Simon Fraser University, Burnaby, BC, Canada V5A-1S6.

‡Now at Institute of Physics, Chinese Academy of Sciences, P.O. Box 603, Beijing 100190, China.

§Now at the Max Planck Institute for the Physics of Complex Systems, Nöthnitzer Str. 38, 01187 Dresden, Germany.

‖Corresponding author: vtripathi@theory.tifr.res.in

observed in α-$RuCl_3$, but no explanation for this feature has yet been found using theoretical calculations [56,57]. Here we show the likely universality of such a peak-dip signature in magnetic torque, as a signature of the field-induced quantum spin liquid (also revealed in the Kitaev system α-$RuCl_3$ at lower energy scales [58–60]), thus placing in a different light the relevance of Kitaev materials in realizing the long-sought-after quantum spin liquid ground state.

Na_2IrO_3 is a layered Mott insulator with an energy gap $E_g = 340$ meV [40] and spin-orbit coupling $\lambda \approx 0.5$ eV [19]. The magnetic susceptibility follows a Curie-Weiss law at high temperatures with $\theta_{CW} \approx -116$ K and an effective Ir moment $\mu_{\text{eff}} = 1.82\mu_B$ [36–38]. The frustrating effects of strong Kitaev correlations cause the suppression of long range order in this material to a Néel temperature ($T_N \approx 15$ K) far below the Curie temperature [39]. Neutron and x-ray diffraction [36], inelastic neutron scattering (INS) [37], and resonant inelastic x-ray scattering (RIXS) [44] measurements reveal the low temperature ordered phase to be an antiferromagnetic zigzag phase with an ordered moment $\mu_{\text{ord}} \approx 0.2\mu_B$ [36–38]. The parameter space of couplings for Na_2IrO_3 has thus far been constrained using *ab initio* computations [16,20,23,24], numerical techniques such as exact diagonalization [18,26,51,61], classical Monte Carlo simulations [17,21], and degenerate perturbation theory [14,15,18,26,51], as well as experimental investigation [37]. Based on such phenomenological justification, the simplest model arrived at is a nearest-neighbor model with a dominant *antiferromagnetic* Kitaev [26,51] and a smaller *ferromagnetic* Heisenberg exchange. In subsequent calculations we refer to this model with dominant antiferromagnetic Kitaev exchange as *Model A*. A different model with a dominant *ferromagnetic* Kitaev and smaller *antiferromagnetic* Heisenberg exchange is however suggested by quantum chemistry [16] and other *ab initio* calculations [20,23,24]. In order to stabilize a zigzag phase within such a model, further neighbor couplings [15–17,24,35] are included in a model we refer to as *Model B*, or additional anisotropic interactions [20] are included in a model we refer to as *Model C*. Here we distinguish between these categories of models with either dominant antiferromagnetic Kitaev, or dominant ferromagnetic Kitaev interactions, by performing measurements of the finite magnetic-field response of Na_2IrO_3 and comparing our results with exact diagonalization simulations.

A single crystal of Na_2IrO_3, of dimension $\approx$100 μm on a side, with a much smaller thickness, was mounted on a piezoresistive cantilever and measured on an *in situ* rotating stage in pulsed magnetic fields up to 60 T. The torque response (τ) was measured as a function of the magnetic field at various fixed angles ($0^\circ \lesssim \theta \lesssim 90^\circ$) of the crystalline axis normal to the honeycomb lattice, with respect to the magnetic-field axis. A distinctive nonmonotonic feature is observed in the magnetic torque response (Fig. 1). A peak in the magnetic torque in the vicinity of 30–40 T is followed by a dip in the vicinity of 45–55 T. The peak and dip features are separated by as much as $\approx$15 T near $\theta \approx 45^\circ$–55°, but draw closer together at angles closer to $\theta \approx 0^\circ$ and $\theta \approx 90^\circ$. In the vicinity of $\theta \approx 0^\circ$ and $\theta \approx 90^\circ$, the peak and dip features are seen to merge into a single plateaulike feature. This evolution of the signature peak-dip feature as a function

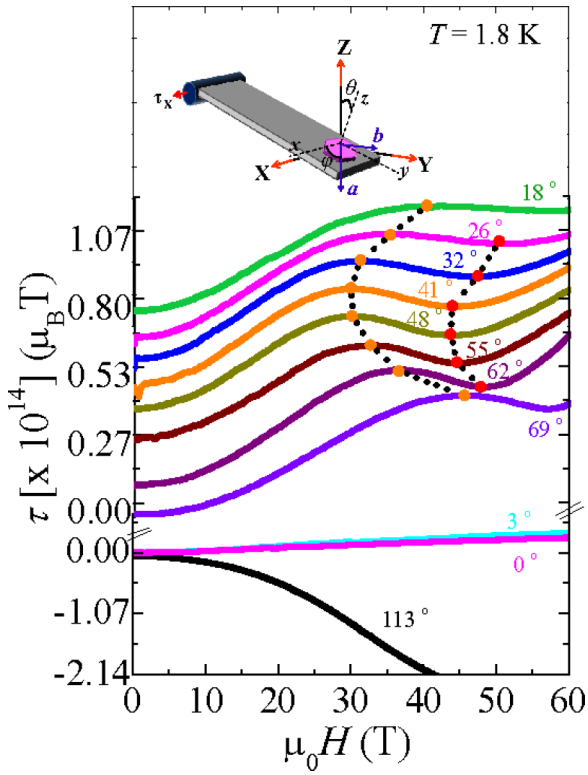

FIG. 1. Magnetic torque (τ) measured as a function of magnetic field for different polar angular orientations (θ) and azimuthal angle $\phi = 90^\circ$. A peak dip structure is observed in the magnetic torque, and is seen to evolve with θ. Individual torque curves have been offset for clarity. (Inset: a crystal on the cantilever with the various coordinate systems: $XYZ \rightarrow$ lab frame; $xyz \rightarrow$ frame fixed to the cantilever, so that X and x coincide. θ is the angle that the normal to the crystal makes with the magnetic field, and the measured magnetic torque along the X direction is referred to as τ.)

of field-inclination angle and magnetic field is shown in Fig. 2 for two different azimuthal orientations ($\phi = 0^\circ, 90^\circ$), where ϕ is the angle that the crystallographic a axis makes with the axis of rotation of the cantilever. The high magnetic-field torque response of Na_2IrO_3 was independently measured for two crystals, for three different azimuthal orientations ($\phi = 0^\circ$, 90°, and 180°), at a temperature of 1.8 K and results for both were found to be very similar [62]. The signature peak-dip feature is found to disappear above the zigzag ordering temperature [62]. Meanwhile, the isotropic magnetization (m_Z) measured using an extraction magnetometer in pulsed magnetic fields up to 60 T, and a force magnetometer in steady fields up to 30 T [63], is found to be largely featureless and to increase linearly with magnetic field up to 60 T [62].

We use theoretical modeling of the nonmonotonic features we observe in the high field torque response to distinguish between potential microscopic models. Our starting point is the usual spin Hamiltonian [14,26] with nearest-neighbor Kitaev and Heisenberg interactions:

$$J_{\text{h}} \sum_{\langle ij \rangle} \vec{\sigma_i} \cdot \vec{\sigma_j} + J_{\text{K}} \sum_{\langle ij \rangle} \sigma_i^\gamma \sigma_j^\gamma, \qquad (1)$$

where $\gamma = x, y, z$ labels an axis in spin space and a bond direction of the honeycomb lattice, and the Hamiltonian is

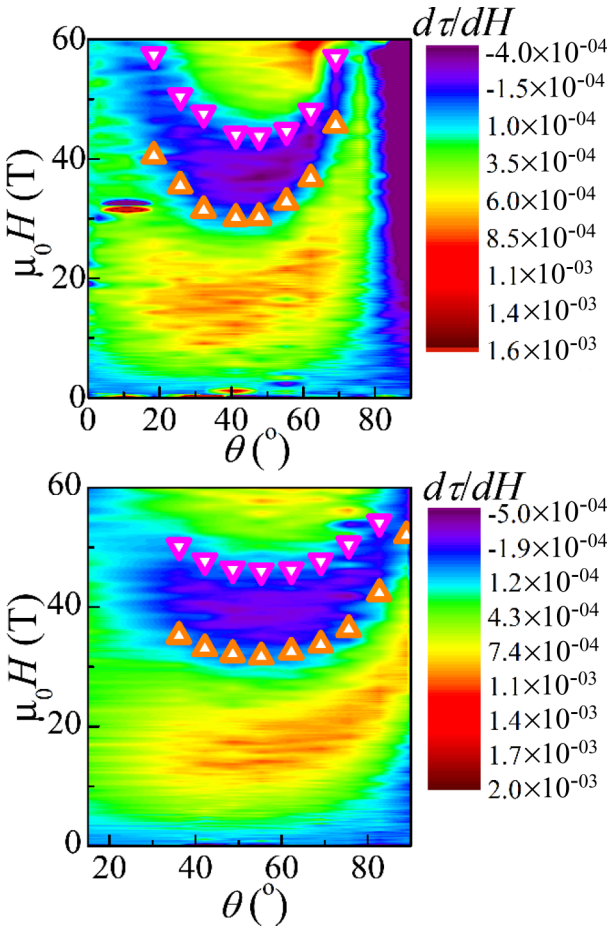

FIG. 2. Derivative of experimentally measured magnetic torque with respect to magnetic field ($\frac{d\tau}{dH}$) as a function of magnetic field and angle (θ) for $\phi = 90^\circ$ (top) and $\phi = 0^\circ$ (bottom). The position of the maxima in the torque is indicated by regular triangles, while that of the subsequent minima is marked by inverted triangles.

expressed in terms of Pauli matrices $\vec{\sigma_i}$. *Model A* with dominant antiferromagnetic Kitaev interactions is parametrized by nearest-neighbor interactions $J_h < 0$ and $J_K > 0$. In *Model B*, further neighbor antiferromagnetic Heisenberg couplings J_2 and J_3 [15] are introduced up to the third nearest neighbor, with $J_h > 0$ and $J_K < 0$. In *Model C*, bond-dependent nearest-neighbor symmetric off-diagonal terms $H_{\rm od}^{(\gamma)} = \Gamma \sum_{\alpha\neq\beta\neq\gamma} \sum_{\{i,j\}} (\sigma_i^\alpha \sigma_j^\beta + \sigma_i^\beta \sigma_j^\alpha)$ (where α and β are the two remaining directions apart from the Kitaev bond direction γ) [51] and $H'_{\rm od} = \Gamma' \sum_{\alpha\neq\beta\neq\gamma} \sum_{\{i,j\}} (\sigma_i^\beta \sigma_j^\gamma + \sigma_i^\gamma \sigma_j^\beta + \sigma_i^\alpha \sigma_j^\gamma + \sigma_i^\gamma \sigma_j^\alpha)$ [18] accounting for trigonal distortions of the oxygen octahedra are introduced. The main parameters of these models are summarized in Table I.

For our calculations, we use a hexagonal 24-site cluster [14,18,26,51] with periodic boundary conditions. The effect of the applied magnetic field $\vec{H} = H\hat{z}$ (in the laboratory frame) on the system is described by $H_{\rm mag} = (\frac{g}{2}) \sum_i \sum_\gamma h_\gamma \sigma_i^\gamma$, with $g \approx 1.78$ [26] being the Lande g factor, assumed to be a constant, and $\vec{h} = (h_x, h_y, h_z)$ being the field as expressed in the crystal octahedron frame. Exact diagonalization calculations for the ground state energy and eigenvector are performed using a modified Lanczos algorithm [64]. The code was benchmarked by reproducing the results in [26]. The chosen parameters are further verified to be consistent with the zigzag ground state of Na_2IrO_3 by calculating the structure factors $S(\vec{Q})$ [18,51,54,65,66] for zigzag, stripy, ferromagnetic, and antiferromagnetic ground states [62].

TABLE I. Models considered for exact diagonalization calculations, where J_h refers to the nearest-neighbor Heisenberg interaction, J_K refers to the Kitaev interaction, J_2 and J_3 refer to further-neighbor Heisenberg terms, and Γ and Γ' refer to symmetric off-diagonal exchange interactions.

Model	J_h	J_K	J_2	J_3	Γ	Γ'
Antiferromagnetic Kitaev (*Model A*)	−	+	×	×	×	×
Ferromagnetic Kitaev (*Model B*)	+	−	+	+	×	×
Ferromagnetic Kitaev (*Model C*)	+	−	×	×	+	−

The calculated magnetic torque responses for the different models are shown in Figs. 3 and 4. We find the peak-dip feature in the magnetic torque response to be reproduced only by models with dominant ferromagnetic Kitaev interactions (i.e., *Models B and C*), whereas models with dominant antiferromagnetic Kitaev interactions (i.e., *Model A*) display instead a monotonic increase in the magnetic torque with magnetic field. Figure 5 shows the evolution of the peak-dip feature as a function of the field-inclination angle and the magnetic field for *Model B*, calculated using exact diagonalization. We have performed exact diagonalization simulations for magnetic fields up to 300 T for *Model A* (for the parameters used in Fig. 4), and found a single peak in the magnetic torque response at a magnetic field slightly lower than 150 T, beyond which the torque decreases with increase in field strength and no further features are observed. We have also considered variants of *Model A* with isotropic J_2 and J_3 as well

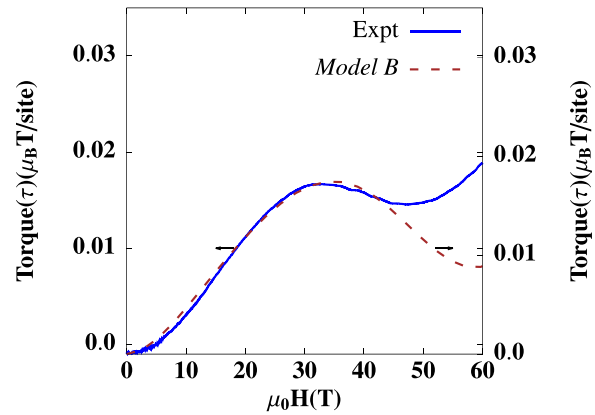

FIG. 3. Magnetic torque as a function of magnetic field (in μ_BT per site) for *Model B* (denoted by τ_B) with parameters $J_h = 3.6$, $J_K = -30.0$ (in meV) for antiferromagnetic Heisenberg and dominant ferromagnetic Kitaev correlations, corresponding to the orientation $\theta = 42^\circ$, $\phi = 0^\circ$. In this case, further neighbor interactions $J_2 = 0.6$, $J_3 = 1.8$ (in meV) are necessary to stabilize a zigzag ground state. The experimental data (solid line) for this orientation is plotted along with the torque response (dashed line) calculated for this model for comparison.

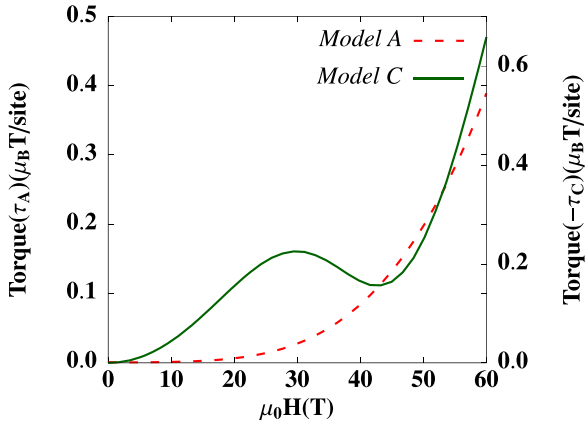

FIG. 4. Magnetic torque calculated as a function of magnetic field (in μ_BT per site) for *Model A* (denoted by τ_A) with parameters $J_h = -4.0$, $J_K = 21.0$ (in meV) for ferromagnetic Heisenberg and dominant antiferromagnetic Kitaev interactions, corresponding to the orientation $\theta = 36^\circ$, $\phi = 0^\circ$, and for *Model C* (denoted by τ_C) with parameters $J_h = 4.0$, $J_K = -16.0$, $\Gamma = 2.4$, and $\Gamma' = -3.2$ (in meV) for antiferromagnetic Heisenberg and dominant ferromagnetic Kitaev exchange, corresponding to the same orientation. In *Model A* (dashed line) characterized by a stable zigzag phase [16,35], no peak-dip feature appears, unlike experimental observations. In contrast, in *Model C* (solid line), where a fine-tuned zigzag phase requires the introduction of nearest-neighbor anisotropic terms Γ and Γ' [18], the magnetic-field dependence of magnetic torque shows a peak-dip feature corresponding with experiment.

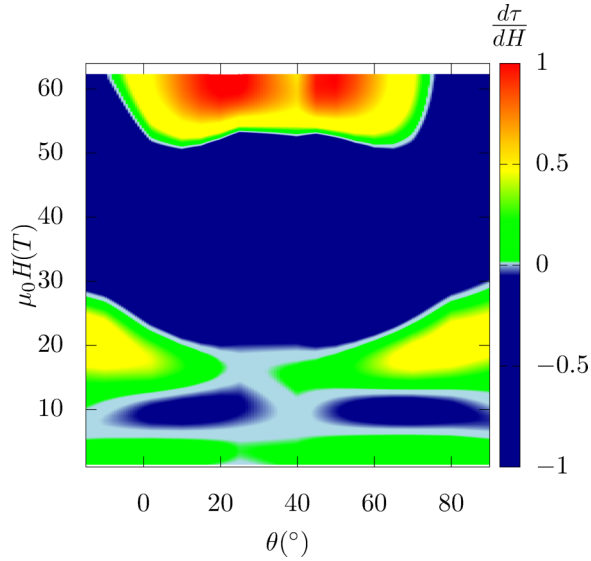

FIG. 5. Calculated contour plot of $\frac{d\tau}{dH}$ in the $\theta - H$ plane, for parameters $J_h = 3.6$, $J_K = -18.0$, $J_2 = 2.4$, and $J_3 = 1.8$ (in meV), i.e., *Model B*, corresponding to the azimuthal angle $\phi = 20^\circ$. We find that the position of the peak-dip feature, indicated by the regions where $\frac{d\tau}{dH}$ changes sign, shifts closer to the origin for increasing (decreasing) values of the polar angle θ for θ close to 0° (90°), in agreement with the experimental results. At the extreme values of θ, the width of the region of nonmonotonicity increases, which is at variance with experiment. The torque values obtained in our simulations can be negative, and in such cases we plot $-\frac{d\tau}{dH}$ instead.

as anisotropic Γ and Γ' terms, and have confirmed that this model does not give a peak-dip feature in its torque response, even with such additional terms present (please refer to Table I in the Supplemental Material [62] for a summary of the different variants considered, and the corresponding torque curves).

Our results strongly indicate that Na_2IrO_3 is described by a model dominated by ferromagnetic Kitaev exchange. The distinctive peak-dip feature in the torque response thus provides an independent handle for constraining experimental data. We note that classical Monte Carlo simulations were unable to reproduce the peak-dip feature, underlining the importance of quantum effects in this material, as has also been emphasized in the recent literature [55]. Of the two types of ferromagnetic Kitaev exchange models we consider, in *Model B*, the peak-dip feature is observed over a large parameter range (in fact, larger than the space over which a zigzag ground state is seen), while in *Model C*, the peak-dip feature only appears upon inclusion of a significant $\Gamma' < 0$ term, which physically is associated with trigonal distortion in Na_2IrO_3. The inclusion of significant anisotropy terms in *Model B* does not yield additional peak-dip features, with the peak-dip surviving only for relatively small values of additional anisotropic interactions. *Models B* and *C* can thus potentially be distinguished by high magnetic-field torque magnetometry measurements on chemically doped Na_2IrO_3 with various extents of trigonal distortion, which should have an observable effect on the peak-dip feature.

We compute the evolution of the spin correlation functions with distance for increasing magnetic-field values. The extent of decay of the correlation functions with distance reveals the presence or absence of long range correlations in the high field regime. The correlation functions $C_{ij} = \langle (\vec{\sigma_i} - \langle \vec{\sigma_i} \rangle) \cdot (\vec{\sigma_j} - \langle \vec{\sigma_j} \rangle) \rangle$ are calculated for a chosen set of neighboring sites in the 24-site cluster, and plotted in Fig. 6 as a function of $\frac{|i-j|}{a}$ (a being the distance between nearest neighbor sites) for

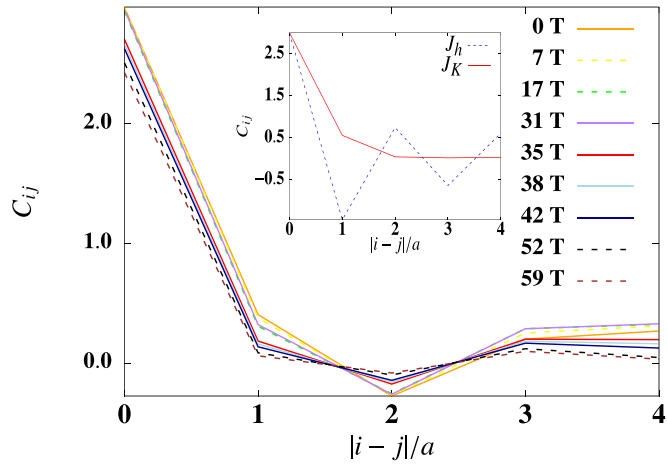

FIG. 6. Correlation functions C_{ij} calculated as a function of $\frac{|i-j|}{a}$, a being the distance between two neighboring sites, with parameters $J_h = 4.0$, $J_K = -16.0$, $\Gamma = 2.4$, and $\Gamma' = -3.2$ (in meV), for an orientation of $\theta = 36^\circ$, $\phi = 0^\circ$. The inset shows the corresponding plots for a pure Heisenberg model with $J_h = 16.0$ meV (blue) and for a pure Kitaev model with $J_K = -16.0$ meV (red). It can be clearly seen that for higher fields (>35 T), the correlation functions fall rapidly with distance and behave more and more like those of a pure Kitaev model, characterized by a spin liquid ground state.

different values of the applied magnetic field. We find that the decay of the correlation functions C_{ij} as a function of $\frac{|i-j|}{a}$ is much faster at relatively higher values of the applied field, and the amplitude of the oscillation of the correlation functions falls off rapidly with increasing fields, in particular above the zigzag ordering scale. Furthermore, structure factor calculations do not show a crossover from antiferromagnetic zigzag order to any of the known ordered states at the position of the metamagnetic transition manifested through the peak dip in the transverse magnetization. Indications therefore are that the high magnetic-field regime beyond the peak-dip feature manifests spin-liquid physics in Na_2IrO_3.

Intriguingly, excitations characteristic of a magnetic-field-induced spin liquid phase [54,58,60,67,68] have also been reported in the Kitaev system α-$RuCl_3$. Our work sheds light on the universality of magnetic-field-induced quantum spin liquid physics in Kitaev systems, which we find to be signaled by the peak dip structure in the anisotropic magnetization at the zigzag ordering scale, also recently reported in α-$RuCl_3$ [56]. Recent calculations in α-$RuCl_3$ [52,53] based on experimental measurements such as electron energy loss spectroscopy and thermal conductivity also favor a dominant ferromagnetic Kitaev model. The striking similarities between these two materials indicates that the experimental features in the magnetoresponse and their theoretical interpretation that we report here are governed by intrinsic Kitaev physics, and are not peculiarities associated with parameters beyond the scope of our model such as interlayer couplings and disorder characteristics, which are expected to be very different for these two materials. The microscopic models we calculate here are thus indicated to be relevant to a broad class of spin-orbit coupled honeycomb Kitaev materials including α-$RuCl_3$, which we find are excellent models to explore the long-sought-after field-induced spin liquid phase.

The authors gratefully acknowledge useful discussions with Giniyat Khaliullin, Itamar Kimchi, Subhro Bhattacharjee, and Steve Winter. We thank E. V. Sampathkumaran for the generous use of facilities for crystal growth. V.T. acknowledges DST for a Swarnajayanti grant (No. DST/SJF/PSA-0212012-13). S.D.D. and S.E.S. acknowledge support from the Royal Society, the Winton Programme for the Physics of Sustainability, and the European Research Council under the European Unions Seventh Framework Programme (Grant No. FP/2007-2013)/ERC Grant Agreement No. 337425. L.B. is supported by DOE-BES through award No. DE-SC0002613. G.C. acknowledges the support of the US National Science Foundation via Grant No. DMR 1712101. A.M. acknowledges the support of the HFML-RU/FOM, member of the European Magnetic Field Laboratory (EMFL). H.Y.K. acknowledges the support of the NSERC of Canada and the center for Quantum Materials at the University of Toronto.

High field experiments were performed by S.D.D. with contributions from Z.Z., E.M., R.D.M., G.L., L.B., and A.M. Theory was developed and calculations performed by S.K. and V.T. with contributions from H.-Y.K. and J.G.R. Single crystal growth was performed by S.D.D. and G.C. The project was conceived and supervised by S.E.S. and V.T. The manuscript was written by S.D.D., S.K., V.T., and S.E.S. with input from all the authors.

[1] K. Ran, J. Wang, W. Wang, Z.-Y. Dong, X. Ren, S. Bao, S. Li, Z. Ma, Y. Gan, Y. Zhang, J. T. Park, G. Deng, S. Danilkin, S.-L. Yu, J.-X. Li, and J. Wen, Phys. Rev. Lett. **118**, 107203 (2017).

[2] L. J. Sandilands, Y. Tian, A. A. Reijnders, H.-S. Kim, K. W. Plumb, Y.-J. Kim, H.-Y. Kee, and K. S. Burch, Phys. Rev. B **93**, 075144 (2016).

[3] L. J. Sandilands, Y. Tian, K. W. Plumb, Y.-J. Kim, and K. S. Burch, Phys. Rev. Lett. **114**, 147201 (2015).

[4] K. W. Plumb, J. P. Clancy, L. J. Sandilands, V. V. Shankar, Y. F. Hu, K. S. Burch, H.-Y. Kee, and Y.-J. Kim, Phys. Rev. B **90**, 041112 (2014).

[5] H.-S. Kim, V. Shankar V., A. Catuneanu, and H.-Y. Kee, Phys. Rev. B **91**, 241110(R) (2015).

[6] H.-S. Kim and H.-Y. Kee, Phys. Rev. B **93**, 155143 (2016).

[7] H. B. Cao, A. Banerjee, J.-Q. Yan, C. A. Bridges, M. D. Lumsden, D. G. Mandrus, D. A. Tennant, B. C. Chakoumakos, and S. E. Nagler, Phys. Rev. B **93**, 134423 (2016).

[8] F. Lang, P. J. Baker, A. A. Haghighirad, Y. Li, D. Prabhakaran, R. Valentí, and S. J. Blundell, Phys. Rev. B **94**, 020407 (2016).

[9] Y. S. Hou, H. J. Xiang, and X. G. Gong, Phys. Rev. B **96**, 054410 (2017).

[10] M. Majumder, M. Schmidt, H. Rosner, A. A. Tsirlin, H. Yasuoka, and M. Baenitz, Phys. Rev. B **91**, 180401(R) (2015).

[11] S. M. Winter, K. Riedl, P. A. Maksimov, A. L. Chernyshev, A. Honecker, and R. Valentí, Nat. Commun. **8**, 1152 (2017).

[12] P. Lampen-Kelley, S. Rachel, J. Reuther, J.-Q. Yan, A. Banerjee, C. A. Bridges, H. B. Cao, S. E. Nagler, and D. Mandrus, Phys. Rev. B **98**, 100403 (2018).

[13] A. Banerjee, C. A. Bridges, J.-Q. Yan, A. A. Aczel, L. Li, M. B. Stone, G. E. Granroth, M. D. Lumsden, Y. Yiu, J. Knolle, S. Bhattacharjee, D. L. Kovrizhin, R. Moessner, D. A. Tennant, D. G. Mandrus, and S. E. Nagler, Nat. Mater. **15**, 733 (2016).

[14] J. Chaloupka, G. Jackeli, and G. Khaliullin, Phys. Rev. Lett. **105**, 027204 (2010).

[15] I. Kimchi and Y.-Z. You, Phys. Rev. B **84**, 180407 (2011).

[16] V. M. Katukuri, S. Nishimoto, V. Yushankhai, A. Stoyanova, H. Kandpal, S. Choi, R. Coldea, I. Rousochatzakis, L. Hozoi, and J. van den Brink, New J. Phys. **16**, 013056 (2014).

[17] Y. Sizyuk, C. Price, P. Wölfle, and N. B. Perkins, Phys. Rev. B **90**, 155126 (2014).

[18] J. G. Rau and H.-Y. Kee, arXiv:1408.4811.

[19] J. G. Rau, E. K.-H. Lee, and H.-Y. Kee, Annu. Rev. Condens. Matter Phys. **7**, 195 (2016).

[20] Y. Yamaji, Y. Nomura, M. Kurita, R. Arita, and M. Imada, Phys. Rev. Lett. **113**, 107201 (2014).

[21] X. Yao, Phys. Lett. A **379**, 1480 (2015).

[22] S. Bhattacharjee, S.-S. Lee, and Y. B. Kim, New J. Phys. **14**, 073015 (2012).

[23] K. Hu, F. Wang, and J. Feng, Phys. Rev. Lett. **115**, 167204 (2015).

[24] K. Foyevtsova, H. O. Jeschke, I. I. Mazin, D. I. Khomskii, and R. Valentí, Phys. Rev. B **88**, 035107 (2013).

[25] H.-C. Jiang, Z.-C. Gu, X.-L. Qi, and S. Trebst, Phys. Rev. B **83**, 245104 (2011).

[26] J. Chaloupka, G. Jackeli, and G. Khaliullin, Phys. Rev. Lett. **110**, 097204 (2013).

[27] A. Shitade, H. Katsura, J. Kuneš, X.-L. Qi, S.-C. Zhang, and N. Nagaosa, Phys. Rev. Lett. **102**, 256403 (2009).

[28] A. A. Vladimirov, D. Ihle, and N. M. Plakida, J. Exp. Theor. Phys. **122**, 1060 (2016).

[29] J. Chaloupka and G. Khaliullin, Phys. Rev. B **92**, 024413 (2015).

[30] T. Takayama, A. Kato, R. Dinnebier, J. Nuss, H. Kono, L. S. I. Veiga, G. Fabbris, D. Haskel, and H. Takagi, Phys. Rev. Lett. **114**, 077202 (2015).

[31] I. I. Mazin, S. Manni, K. Foyevtsova, H. O. Jeschke, P. Gegenwart, and R. Valentí, Phys. Rev. B **88**, 035115 (2013).

[32] J. Reuther, R. Thomale, and S. Trebst, Phys. Rev. B **84**, 100406 (2011).

[33] Y. S. Hou, J. H. Yang, H. J. Xiang, and X. G. Gong, Phys. Rev. B **98**, 094401 (2018).

[34] H.-J. Kim, J.-H. Lee, and J.-H. Cho, Sci. Rep. **4**, 5253 (2014).

[35] Y. Singh, S. Manni, J. Reuther, T. Berlijn, R. Thomale, W. Ku, S. Trebst, and P. Gegenwart, Phys. Rev. Lett. **108**, 127203 (2012).

[36] F. Ye, S. Chi, H. Cao, B. C. Chakoumakos, J. A. Fernandez-Baca, R. Custelcean, T. F. Qi, O. B. Korneta, and G. Cao, Phys. Rev. B **85**, 180403 (2012).

[37] S. Choi, R. Coldea, A. Kolmogorov, T. Lancaster, I. Mazin, S. Blundell, P. Radaelli, Y. Singh, P. Gegenwart, K. Choi *et al.*, Phys. Rev. Lett. **108**, 127204 (2012).

[38] Y. Singh and P. Gegenwart, Phys. Rev. B **82**, 064412 (2010).

[39] S. H. Chun, J.-W. Kim, J. Kim, H. Zheng, C. C. Stoumpos, C. Malliakas, J. Mitchell, K. Mehlawat, Y. Singh, Y. Choi *et al.*, Nat. Phys. **11**, 462 (2015).

[40] R. Comin, G. Levy, B. Ludbrook, Z.-H. Zhu, C. Veenstra, J. Rosen, Y. Singh, P. Gegenwart, D. Stricker, J. N. Hancock *et al.*, Phys. Rev. Lett. **109**, 266406 (2012).

[41] J. P. Clancy, N. Chen, C. Y. Kim, W. F. Chen, K. W. Plumb, B. C. Jeon, T. W. Noh, and Y. J. Kim, Phys. Rev. B **86**, 195131 (2012).

[42] H. Gretarsson, J. Clancy, X. Liu, J. Hill, E. Bozin, Y. Singh, S. Manni, P. Gegenwart, J. Kim, A. Said *et al.*, Phys. Rev. Lett. **110**, 076402 (2013).

[43] H. Gretarsson, J. Clancy, Y. Singh, P. Gegenwart, J. Hill, J. Kim, M. Upton, A. Said, D. Casa, T. Gog *et al.*, Phys. Rev. B **87**, 220407 (2013).

[44] X. Liu, T. Berlijn, W.-G. Yin, W. Ku, A. Tsvelik, Y.-J. Kim, H. Gretarsson, Y. Singh, P. Gegenwart, and J. P. Hill, Phys. Rev. B **83**, 220403(R) (2011).

[45] K. Mehlawat, A. Thamizhavel, and Y. Singh, Phys. Rev. B **95**, 144406 (2017).

[46] A. Banerjee, P. Lampen-Kelly, J. Knolle, C. Balz, A. A. Aczel, B. Winn, Y. Liu, D. Pajerowski, J. Yan, C. A. Bridges, A. T. Savici, B. C. Chakoumakos, M. D. Lumsden, D. A. Tennant, R. Moessner, D. G. Mandrus, and S. E. Nagler, npj Quantum Mater. **3**, 8 (2018).

[47] A. Y. Kitaev, Ann. Phys. (N.Y.) **303**, 2 (2003).

[48] A. Kitaev, Ann. Phys. (N.Y.) **321**, 2 (2006).

[49] G. Jackeli and G. Khaliullin, Phys. Rev. Lett. **102**, 017205 (2009).

[50] B. Kim, H. Jin, S. Moon, J.-Y. Kim, B.-G. Park, C. Leem, J. Yu, T. Noh, C. Kim, S.-J. Oh *et al.*, Phys. Rev. Lett. **101**, 076402 (2008).

[51] J. G. Rau, E. K.-H. Lee, and H.-Y. Kee, Phys. Rev. Lett. **112**, 077204 (2014).

[52] A. Koitzsch, E. Muller, M. Knupfer, B. Buchner, D. Nowak, A. Isaeva, T. Doert, M. Gruninger, S. Nishimoto, and J. v. d. Brink, arXiv:1709.02712.

[53] J. Cookmeyer and J. E. Moore, Phys. Rev. B **98**, 060412 (2018).

[54] R. Yadav, N. A. Bogdanov, V. M. Katukuri, S. Nishimoto, J. van den Brink, and L. Hozoi, Sci. Rep. **6**, 37925 (2016).

[55] L. Janssen, E. C. Andrade, and M. Vojta, Phys. Rev. B **96**, 064430 (2017).

[56] I. A. Leahy, C. A. Pocs, P. E. Siegfried, D. Graf, S.-H. Do, K.-Y. Choi, B. Normand, and M. Lee, Phys. Rev. Lett. **118**, 187203 (2017).

[57] K. Riedl, Y. Li, S. M. Winter, and R. Valenti, arXiv:1809.03943.

[58] J. Zheng, K. Ran, T. Li, J. Wang, P. Wang, B. Liu, Z.-X. Liu, B. Normand, J. Wen, and W. Yu, Phys. Rev. Lett. **119**, 227208 (2017).

[59] L. Y. Shi, Y. Q. Liu, T. Lin, M. Y. Zhang, S. J. Zhang, L. Wang, Y. G. Shi, T. Dong, and N. L. Wang, Phys. Rev. B **98**, 094414 (2018).

[60] D. Hirobe, M. Sato, Y. Shiomi, H. Tanaka, and E. Saitoh, Phys. Rev. B **95**, 241112 (2017).

[61] J. Chaloupka and G. Khaliullin, Phys. Rev. B **94**, 064435 (2016).

[62] See Supplemental Material at http://link.aps.org/supplemental/10.1103/PhysRevB.99.081101 for a description of the experimental details, numerical setup and algorithm, structure factor calculations, and extended modeling over an extensive range of parameter space.

[63] A. McCollam, P. G. van Rhee, J. Rook, E. Kampert, U. Zeitler, and J. C. Maan, Rev. Sci. Instrum. **82**, 053909 (2011).

[64] E. R. Gagliano, E. Dagotto, A. Moreo, and F. C. Alcaraz, Phys. Rev. B **34**, 1677 (1986).

[65] F. Trousselet, G. Khaliullin, and P. Horsch, Phys. Rev. B **84**, 054409 (2011).

[66] Z. Alpichshev, F. Mahmood, G. Cao, and N. Gedik, Phys. Rev. Lett. **114**, 017203 (2015).

[67] J. Sears, Y. Zhao, Z. Xu, J. Lynn, and Y.-J. Kim, Phys. Rev. B **95**, 180411 (2017).

[68] R. D. Johnson, S. C. Williams, A. A. Haghighirad, J. Singleton, V. Zapf, P. Manuel, I. I. Mazin, Y. Li, H. O. Jeschke, R. Valentí, and R. Coldea, Phys. Rev. B **92**, 235119 (2015).